AIAA JOURNAL
Vol. 42, No. 7, July 2004

Static Fields in Magnetoelectroelastic Laminates

Paul R. Heyliger*
Colorado State University, Fort Collins, Colorado 80523
and
Ernian Pan†
University of Akron, Akron, Ohio 44325-3905

The through-thickness elastic, electric, and magnetic fields of laminates composed of elastic, piezoelectric, and magnetostrictive layers are considered under static conditions to determine their fundamental behavior and to investigate the limits of simplified plate theories in which the fields are assumed to possess a specific type of behavior. The weak form of the equations of motion/equilibrium, Gauss's law and Gauss's law for magnetism, are formulated for a rectangular laminate with arbitrary edge boundary conditions under the application of applied surface displacement/traction, electric potential/electric flux, or magnetic potential/magnetic flux. The layers within the laminate are allowed to possess any linear constitutive law consistent with a magnetoelectroelastic solid, and the number of layers is arbitrary. The Ritz method is used in combination with a discrete-layer theory, and approximate solutions for the displacements, electric potential, and magnetic potential are sought to the weak form of the governing equations. The use of linear combinations of through-thickness approximations, along with separate approximations for the in-plane behavior, allows an accurate representation of the break in variable slope across an interface with dissimilar material properties. The model is applied to problems with either known exact solutions or a finite element approximation to the governing equations. Excellent agreement is obtained for all cases.

Nomenclature

$a_{ij}, b_{ik}, c_{ij}, f_{ij}, g_{ij}$	=	layer constants for primary unknowns
B_i	=	components of magnetic flux vector
C_{ij}	=	components of material elastic stiffness tensor
D_i	=	components of electric displacement vector
d_{ij}	=	magnetoelectric coupling coefficients
E_i	=	components of electric field vector
e_{ij}	=	piezoelectric coupling coefficients
f_i	=	components of body force vector
H_i	=	components of magnetic field vector
h	=	total thickness of laminate
K_{ij}	=	coefficients of final discrete-layer coefficient matrix
L_x, L_y	=	edge lengths of laminate in x and y directions
N	=	number of total layers in the laminate
n_i	=	components of unit normal vector on surface
q_{ij}	=	piezomagnetic coupling coefficients
S	=	bounding surface of laminate
u, v, w	=	displacement components of laminate in x, y, and z directions
u_i	=	components of displacement vector
V	=	total volume of laminate
x, y, z	=	rectangular Cartesian coordinates of laminate
$\Gamma_i(x, y)$	=	in-plane approximation functions
$\Gamma_i(z)$	=	thickness approximation functions
γ_i	=	strain tensor components in contracted notation
γ_{ij}	=	elements of infinitesimal strain tensor
δ	=	variational operator
ε_{ij}	=	material dielectric tensor
μ_{ij}	=	material magnetic permeability tensor
σ_{ij}	=	components of Cauchy stress tensor
ϕ	=	electric potential
ψ	=	magnetic potential

Received 1 October 2002; revision received 1 August 2003; accepted for publication 1 August 2003.

*Professor, Department of Civil Engineering; prh@engr.colostate.edu.
†Associate Professor, Department of Civil Engineering.

Introduction

THERE have been numerous studies related to adaptive or smart laminates in the past decade, many of which have dealt with either sensing or actuating structural components by the application of electric and/or magnetic fields to solids with coupled field constitutive behavior. The review paper of Saravanos and Heyliger[1] and the monograph of Tzou[2] give a number of examples of this type of approach when applied to laminated media. Another class of adaptive materials and structures that has seen less development are solids with a combined magnetoelectric effect, in which significant interactions are present between the elastic, electric, and magnetic fields. Several studies have been completed related to these materials, including those of Harshe et al.,[3] Nan,[4] and Benveniste.[5] More recently, several exact solutions for magnetoelectroelastic laminates have been found for the static and free vibration behavior by Pan[6] and Pan and Heyliger.[7] These solutions are highly valuable for the investigation of the basic nature of the field variables, but have thus far been restricted to the case of simple support along the edges of the laminate. A more general method that could be applied to varying edge conditions would be extremely useful in the evaluation of the range of acceptable behavior of simplified plate theories.

In this study, approximate solutions to the weak form of the governing equations of equilibrium/motion, charge, and magnetic flux are obtained for laminates containing layers of potentially magnetoelectroelastic material, in which there can exist elastic displacement fields, the electric potential (or voltage), and the magnetic potential. As the laminate undergoes deformation, there is coupling among these fields and the conversion of energy from one form to another that is captured by consideration of the independent approximations to the three displacement components u_i, the electric potential ϕ, and the magnetic potential ψ. These five variables are treated as layerwise unknowns in an approximate discrete-layer model, in which the through-thickness behavior of the five primary unknown fields

is not assumed a priori but is instead found as a result of the solution process.

The solution approach presented here is not dependent on specific surface or edge boundary conditions, but a primary aim of this study is to determine the relative accuracy of the present approximate model compared to the exact solution. For this reason, emphasis is given to the case of simple support, for which exact solutions are known. This allows a direct study of convergence properties with eventual application to other support conditions.

Problem Statement

The fundamental problem under consideration is a layered rectangular paralellepiped (or plate) with N layers through the vertical or thickness dimension z. Conventional rectangular Cartesian coordinates are used to describe the geometry, with x and y coincident with the planar dimensions of the laminate with corresponding lengths of L_x and L_y. The letter h denotes the total thickness of the laminate. The origin of the coordinate system is located at one of the lower corners of the laminate so that all of the material within the laminate is in positive (x, y, z) territory.

The edge boundary conditions are arbitrary. In most of the examples considered in this study, these are selected to be consistent with those of geometric simple support, that is, the transverse displacement w and tangential displacement along the edge length are both specified to be zero, with zero normal traction also specified along the edge length. In terms of the electric and magnetic field variables, the edges are fixed at zero for both ϕ and ψ, but nonzero fields can be specified along the top and bottom surfaces of the laminate. The general boundary conditions along these two surfaces depend on the problem being studied, and are discussed in the sequel.

Theory

Governing Equations

Within the laminate, there are body forces but no electric charge or current densities. Under these conditions, the equations of equilibrium are given by

$$\sigma_{ij,j} + f_i = 0 \tag{1}$$

Here σ_{ij} are the components of stress and f_i are the components of the body force vector. Gauss's law in the absence of charge density can be expressed in terms of the electric displacement vector components D_i as

$$D_{i,i} = 0 \tag{2}$$

Gauss's law for magnetism enforces the lack of existence of magnetic monopoles and can be written as

$$B_{i,i} = 0 \tag{3}$$

where B_i are the components of the magnetic flux vector.

The coupled constitutive laws for a linear anisotropic magneto-electroelastic material can be written as

$$\sigma_i = C_{ik}\gamma_k - e_{ki}E_k - q_{ki}H_k, \qquad D_i = e_{ik}\gamma_k + \varepsilon_{ik}E_k + d_{ik}H_k$$
$$B_i = q_{ik}\gamma_k + d_{ik}E_k + \mu_{ik}H_k \tag{4}$$

Here, C_{ij}, ε_{ij}, and μ_{ij} are components of the elastic stiffness tensor, the dielectric permeability, and the magnetic permeability, respectively; e_{ij}, q_{ij}, and d_{ij} are the elements of the piezoelectric, piezomagnetic, and magnetoelectric coefficients, respectively; and γ_i, E_i, and H_i are the components of the linear strain tensor and the electric and magnetic field vectors, respectively. The latter three measures are defined by the gradient relations

$$\gamma_{ij} = \tfrac{1}{2}(u_{i,j} + u_{j,i}), \qquad E_i = -\phi_{,i}, \qquad H_i = -\psi_{,i} \tag{5}$$

where u_i, ϕ, and φ are the displacement vector components, electric, and magnetic potentials, respectively. Here the standard contracted notation has been used to reduce the number of subscripts for each of the tensor representations, for example, $\gamma_1 = \gamma_{11}$ and $\gamma_4 = \gamma_{23}$.

The nonzero terms for the orthotropic material property tensors can be expressed in matrix form as follows:

$$[C] = \begin{bmatrix} C_{11} & C_{12} & C_{13} & 0 & 0 & 0 \\ C_{12} & C_{22} & C_{23} & 0 & 0 & 0 \\ C_{13} & C_{23} & C_{33} & 0 & 0 & 0 \\ 0 & 0 & 0 & C_{44} & 0 & 0 \\ 0 & 0 & 0 & 0 & C_{55} & 0 \\ 0 & 0 & 0 & 0 & 0 & C_{66} \end{bmatrix}$$

$$[q] = \begin{bmatrix} 0 & 0 & 0 & 0 & q_{15} & 0 \\ 0 & 0 & 0 & q_{24} & 0 & 0 \\ q_{31} & q_{32} & q_{33} & 0 & 0 & 0 \end{bmatrix}$$

$$[e] = \begin{bmatrix} 0 & 0 & 0 & 0 & e_{15} & 0 \\ 0 & 0 & 0 & e_{24} & 0 & 0 \\ e_{31} & e_{32} & e_{33} & 0 & 0 & 0 \end{bmatrix}$$

$$[\varepsilon] = \begin{bmatrix} \varepsilon_{11} & 0 & 0 \\ 0 & \varepsilon_{22} & 0 \\ 0 & 0 & \varepsilon_{33} \end{bmatrix}, \qquad [\mu] = \begin{bmatrix} \mu_{11} & 0 & 0 \\ 0 & \mu_{22} & 0 \\ 0 & 0 & \mu_{33} \end{bmatrix}$$

$$[d] = \begin{bmatrix} d_{11} & 0 & 0 \\ 0 & d_{22} & 0 \\ 0 & 0 & d_{33} \end{bmatrix} \tag{6}$$

Materials with different symmetries can be considered with this representation. Although other types of material tensor properties could be considered, only materials that possess transverse isotropy are considered in this study. The numerical values for each of the material parameters are given for the specific examples in the sections that follow.

Variational Formulation

Exact solutions to the foregoing equations are rare and can typically only be obtained for very specific boundary conditions. In this study, a more general solution approach is developed for a variety of boundary conditions. This approach is based on a solution of the weak form of the equations just given. This is accomplished by multiplication of each of the three governing differential equations by a sufficiently differentiable weight function that has the physical meaning of a virtual displacement, electric potential, and magnetic potential, respectively. The result is then set equal to zero.[8] These are expressed as

$$0 = \int_V \delta u_i(\sigma_{ij,j} + f_i)\,\mathrm{d}V, \qquad 0 = \int_V \delta\phi(D_{i,i})\,\mathrm{d}V$$
$$0 = \int_V \delta\psi(B_{i,i})\,\mathrm{d}V \tag{7}$$

Next, each of these three equations is integrated by parts to transfer the spatial differential operator off of the flux variable and on to the weight function. Completion of this operation and the use of the divergence theorem yields the final weak form of the governing equations as

$$0 = \int_V (\sigma_{ij}\delta\gamma_{ij} + \delta u_i f_i)\,\mathrm{d}V - \oint_S \sigma_{ij}n_j\delta u_i\,\mathrm{d}s$$
$$0 = \int_V (D_j\delta\phi_{,j})\,\mathrm{d}V - \oint_S D_j n_j\delta\phi\,\mathrm{d}s$$
$$0 = \int_V (B_j\delta\psi_{,j})\,\mathrm{d}V - \oint_S B_j n_j\delta\psi\,\mathrm{d}s \tag{8}$$

We then substitute in the constitutive and field-potential relations to give the final weak form in terms of the three displacement components and the two potentials.

Discrete-Layer Approximations

Approximations to the three displacement components, the electric potential, and the magnetic potential are sought by separation of the nature of the field behavior into through-thickness and in-plane behaviors. We use approximations that split the through-thickness behavior and the planar behavior of the laminate into separate functions, allowing for significant freedom in the behavior of the fields within the laminate. Such an approach was first applied to piezoelectric laminates by Pauley and Dong[9] and has been generalized for elastic laminates by Reddy.[10] The approximations can be written as

$$u(x, y, z) = a_{ij} \sum_i \Gamma_i^u(z) \sum_j \Gamma_j^u(x, y)$$

$$v(x, y, z) = b_{ij} \sum_i \Gamma_i^v(z) \sum_j \Gamma_j^v(x, y)$$

$$w(x, y, z) = c_{ij} \sum_i \Gamma_i^w(z) \sum_j \Gamma_j^w(x, y)$$

$$\phi(x, y, z) = f_{ij} \sum_i \Gamma_i^\phi(z) \sum_j \Gamma_j^\phi(x, y)$$

$$\varphi(x, y, z) = g_{ij} \sum_i \Gamma_i^\psi(z) \sum_j \Gamma_j^\psi(x, y) \tag{9}$$

Here, the elements a_{ij}, b_{ij}, c_{ij}, f_{ij}, and g_{ij} are constants associated with the ith layer of the approximation in the laminate along with the jth in-plane approximation to that specific variable. The functions $\Gamma(z)$ represent the one-dimensional through-thickness approximation functions, whereas $\Gamma(x, y)$ represent the in-plane approximations in x and y. There is an individual constant that multiples the contribution of each of the terms used to approximate each of the five field variables within the laminate at each layer interface. Note that a numerical/approximation layer needs not be exactly the same as a physical layer.

Substitution in the form of approximation for the remaining field variables allows the expression of the weak form of the governing equations in matrix form as given by the following linear system of equations:

$$\begin{bmatrix} [K_{11}] & [K_{12}] & [K_{13}] & [K_{14}] & [K_{15}] \\ [K_{21}] & [K_{22}] & [K_{23}] & [K_{24}] & [K_{25}] \\ [K_{31}] & [K_{32}] & [K_{33}] & [K_{34}] & [K_{35}] \\ [K_{41}] & [K_{42}] & [K_{43}] & [K_{44}] & [K_{45}] \\ [K_{51}] & [K_{52}] & [K_{53}] & [K_{54}] & [K_{55}] \end{bmatrix} \begin{Bmatrix} \{a\} \\ \{b\} \\ \{c\} \\ \{f\} \\ \{g\} \end{Bmatrix} = \begin{Bmatrix} \{f_1\} \\ \{f_2\} \\ \{f_3\} \\ \{f_4\} \\ \{f_5\} \end{Bmatrix} \tag{10}$$

The elements of these equations are given in the Appendix. These are solved for the coefficients of the approximation functions, allowing one to compute both the primary (displacements and the two potentials) and secondary (stresses, electric displacements, and magnetic fluxes) unknowns at any location within the laminate.

Numerical Examples and Discussion

The primary focus of this study is to introduce the enclosed approximate model as an alternative to the far more cumbersome and restrictive exact solution approach. This latter task, although extremely valuable, is limited to very specific sets of plate boundary conditions. As an initial focus, examples are considered for problems that have been studied by the use of an exact approach by Pan[6] and Pan and Heyliger[7] for the case of static and free vibration of simply supported plates.

To validate the present model initially, results have been compared with exact solutions for the static loading results of elastic plates and for the exact static and free vibration exact solutions for piezoelectric laminates found by Heyliger.[11] Heyliger et al.,[12] and Heyliger.[13] All results are in excellent agreement with the results presented in these studies.

Table 1 Material properties and units for the two materials used in numerical examples

Parameter	$CoFe_2O_4$	$BaTiO_3$
$C_{11} = C_{22}$, GPa	286.0	166.0
C_{33}	269.5	162.0
$C_{13} = C_{23}$	170.5	78.0
C_{12}	173.0	77.0
$C_{44} = C_{55}$	45.3	43.0
C_{66}	56.5	44.5
$e_{31} = e_{32}$, C/m^2	0.0	−4.4
e_{33}	0.0	18.6
$e_{24} = e_{15}$	0.0	11.6
$q_{31} = q_{32}$, N/Am	580.3	0.0
q_{33}	699.7	0.0
$q_{24} = q_{15}$	550.0	0.0
$\varepsilon_{11} = \varepsilon_{22}$, 10^{-9} C^2/(Nm^2)	0.080	11.2
ε_{33}	0.093	12.6
$d_{11} = d_{22}$	0.0	0.0
d_{33}	0.0	0.0
$\mu_{11} = \mu_{22}$, 10^{-6} Ns^2/C^2	−590.0	5.0
μ_{33}	157.0	10.0

Two different materials are studied in the examples that follow. The first is the much-studied piezoelectric solid $BaTiO_3$, and the second is the purely magnetostrictive material $CoFe_2O_4$. The material properties for both of these solids are given in Table 1 along with the appropriate units for each.[14]

Simply Supported Plate

The first problem considered is a square plate under simple support with dimensions of $L_x = L_y = 1$ and $h = 0.3$ (all dimensions in meters) to compare with the exact solution of Pan.[6] The loading is a positive normal traction in the positive z direction on the upper face of the laminate that has the form

$$t_z = t_0 \sin(\pi x/L_x) \sin(\pi y/L_y) \tag{11}$$

where $t_0 = 1$ N/m^2 for this example. All other tractions on the top and bottom surfaces of the laminate are zero, and the electric displacement and magnetic fluxes are also both specified to be zero at the top and bottom surfaces of the laminate. The conditions along the laminate edges are specified as discussed earlier.

The in-plane approximation functions for each of the five field variables are given in the form

$$\Gamma_j^u(x, y) = \cos px \sin qy, \qquad \Gamma_j^v(x, y) = \sin px \cos qy$$

$$\Gamma_j^w(x, y) = \sin px \sin qy, \qquad \Gamma_j^\phi(x, y) = \sin px \sin qy$$

$$\Gamma_j^\psi(x, y) = \sin px \sin qy \tag{12}$$

where $p = n\pi/L_x$ and $q = m\pi/L_y$. Here, the index j is a single integer that is linked to the numbers used for p and q in each of the terms. For the loading considered here, only a single term needs to be used to match the exact solution, that is, the double-sine function for the surface traction, because the fields with $m = n = 1$ identically satisfy the (x, y) dependence of all five field variables. The primary intent of these examples is to show the basic field behavior and to determine the level of convergence in the number of discrete-layers used to represent the laminate.

Single-Layer Magnetostrictive Plate

The first example considered is a single-ply, homogeneous plate of the magnetostrictive $CoFe_2O_4$. The plate is divided into a sequentially higher number of layers starting with 3, 6, and 12 discrete layers. Hence, the size of the resulting matrices to be solved are 20,

Table 2 In-plane displacement $u = v$ (10^{-11} m) at $(0, L_y/2)$ for homogeneous magnetostrictive $CoFe_2O_4$ with simple support under transverse load

z	0.0	0.1	0.2	0.3
$N = 3$	0.29136	0.10078	−0.03877	−0.24628
$N = 6$	0.31166	0.10582	−0.04451	−0.26803
$N = 12$	0.31761	0.10731	−0.04618	−0.27437
Exact	0.31968	0.10782	−0.04676	−0.27657

Table 3 Transverse displacement w (10^{-11} m) at $(L_x/2, L_y/2)$ for homogeneous magnetostrictive $CoFe_2O_4$ plate with simple support under transverse load

z	0.0	0.1	0.2	0.3
$N = 3$	0.86781	0.95044	0.98053	0.95524
$N = 6$	0.90758	0.99128	1.0215	0.99533
$N = 12$	0.91927	1.0033	1.0336	1.0071
Exact	0.92335	1.0076	1.0378	1.0112

Table 4 Magnetic potential ψ (10^{-5} C/s) at $(L_x/2, L_y/2)$ for homogeneous magnetostrictive $CoFe_2O_4$ plate with simple support under transverse load

z	0.0	0.1	0.2	0.3
$N = 3$	−0.50251	−0.50299	−0.29479	−0.010826
$N = 6$	−0.51399	−0.49369	−0.27353	0.7×10^{-4}
$N = 12$	−0.51814	−0.49170	−0.26784	0.3×10^{-2}
Exact	−0.51965	−0.49108	−0.26590	0.4×10^{-2}

35, and 65 for these three cases. In each case we compare our results with those of the exact solution.

The in-plane displacements are shown in Table 2 as a function of thickness position and number of discrete layers. Because this material has transverse isotropy, the u and v displacement fields are identical. The values shown are the maximum quantities for the displacements located at the edges of the plate. Because of the nature of the loading, both of these displacements are zero at the plate center.

In elementary plate theory, the in-plane displacements at the top and bottom surfaces of the plate are identical because the Kirchhoff hypothesis requires that the displacements u and v are linear functions of z. The present model is based on an elasticity approach, however, and it is seen that there is a difference of over 10% between the values at the top and bottom surfaces of the layer. It is also clear that even for a fairly small number of layers, that is, six, the present results are well within 5% error of the exact solution values. This plate is fairly thick, with an L/h ratio of 3.33, and it is highly probable that for thinner plates an even smaller number of layers would be required to achieve similar accuracy.

The behavior of the transverse displacement w is shown in Table 3 by the use of a similar format. Once again, the present results are in excellent agreement with the exact solution. In elementary plate theory, it is common to assume that the displacement field is constant in z, that is, it does not vary through the thickness. From these results, it is clear that, even for a thick plate, this is not an excessively restrictive assumption, with a difference of less than 10% between values at the top and bottom surfaces. As before, a fairly small number of layers well represents the global plate behavior, with the three-layer discretization yielding values within 7% of the exact displacements.

There is no coupling between the magnetoelastic fields and the electric fields for this problem, and the electric potential is identically equal to zero over the entire plate. However, the coupling between the elastic and magnetic field results in a nonzero magnetic potential (and, hence, magnetic field) through the laminate thickness. This distribution is shown in Table 4 as a function of laminate thickness and number of layers in the approximation. The agreement is excellent with the exact solution, although the errors are much higher at the top surface for a small number of layers, and a relatively large number of layers is required to achieve accuracy of a similar level to those of the displacement components. For this example, the present model yields excellent results for the displacement components using a fairly small number of layers. Because of the somewhat large number of layers required for an accurate representation of the magnetic potential, assumptions related to simplified behavior of the variable for thick plates requires careful consideration.

Three-Layer Composite Laminate

The second geometry considered is a three-layer composite laminate formed of the two materials discussed earlier: the piezoelectric $BaTiO_3$ (denoted by the letter B in the sequel) and the magnetostrictive $CoFe_2O_4$ (denoted by the letter F). The laminate geometry is identical to that considered earlier, except that three dissimilar layers are used through the thickness, with equal layer thicknesses used for each lamina. The loading and general form of the boundary conditions and approximation functions are the same as those considered in the preceding example.

In Tables 5–8, the in-plane displacement, transverse displacement, electric potential, and magnetic potential are shown at the top and bottom surfaces of the laminate and at the interface locations between dissimilar layers as a function of number of total layers for an $F/B/F$ laminate. The value of $N = 3$ is the minimum number that could be rationally used for this type of structure because each geometric layer requires at least one discrete layer to represent the material behavior. The convergence is rapid, and even the magnetic potential behavior is well-represented by a relatively small number of layers. Although not shown in Tables 5–8, the discrete-layer model has a significant advantage over other types of plate theories

Table 5 In-plane displacement $u = v$ (10^{-11} m) at $(0, L_y/2)$ for three-layer laminate $F/B/F$ with simple support under transverse load

z	0.0	0.1	0.2	0.3
$N = 3$	0.28912	0.10877	−0.05121	−0.24664
$N = 6$	0.30727	0.11262	−0.05594	−0.26627
$N = 12$	0.31256	0.11374	−0.05730	−0.27194
Exact	0.31440	0.11414	−0.05777	−0.27392

Table 6 Transverse displacement w (10^{-11} m) at $(L_x/2, L_y/2)$ for three-layer laminate $F/B/F$ with simple support under transverse load

z	0.0	0.1	0.2	0.3
$N = 3$	0.83204	0.91605	0.94883	0.92107
$N = 6$	0.86773	0.95121	0.98508	0.95721
$N = 12$	0.87814	0.96269	0.99571	0.96774
Exact	0.88176	0.96638	0.99940	0.97140

Table 7 Electric potential ϕ (10^{-2} V) at $(L_x/2, L_y/2)$ for three-layer laminate $F/B/F$ with simple support under transverse load

z	0.0	0.1	0.2	0.3
$N = 3$	0.37262	0.40518	0.45955	0.42262
$N = 6$	0.37886	0.41160	0.46593	0.42887
$N = 12$	0.38077	0.41360	0.46792	0.43079
Exact	0.38146	0.41431	0.46863	0.43147

Table 8 Magnetic potential ψ (10^{-5} C/s) at $(L_x/2, L_y/2)$ for three-layer laminate $F/B/F$ with simple support under transverse load

z	0.0	0.1	0.2	0.3
$N = 3$	−0.22713	−0.31813	−0.41738	−0.18629
$N = 6$	−0.21916	−0.29835	−0.39320	−0.17621
$N = 12$	−0.21730	−0.29314	−0.38689	−0.17381
Exact	−0.21670	−0.29138	−0.38477	−0.17302

in that the requirement of, say, traction continuity (which implies discontinuity of shear strain and, therefore, through-thickness displacement gradient) is modeled as a matter of course. Allowance of the through-thickness approximations to be discontinuous in slope across an interface captures the exact behavior of these fields, frequently leading to more accurate results. Also of interest is the behavior of the stresses, electric displacement, and magnetic flux components through the laminate thickness. In the text that follows, these quantities are shown for the $B/F/B$ and $F/B/F$ lamination schemes.

In Figs. 1 and 2, the in-plane normal stress σ_{xx} and the transverse shear stress σ_{xz} are shown as a function of laminate thickness for 3, 6, 12, and 24 layers and are compared with the exact solution of Pan.[6] The normal stress component is discontinuous at the dissimilar layer interface, and, hence, there is a slight break in magnitude caused by the difference material properties and displacement gradient across the interface. For the $B/F/B$ laminate, there is an increase in stress

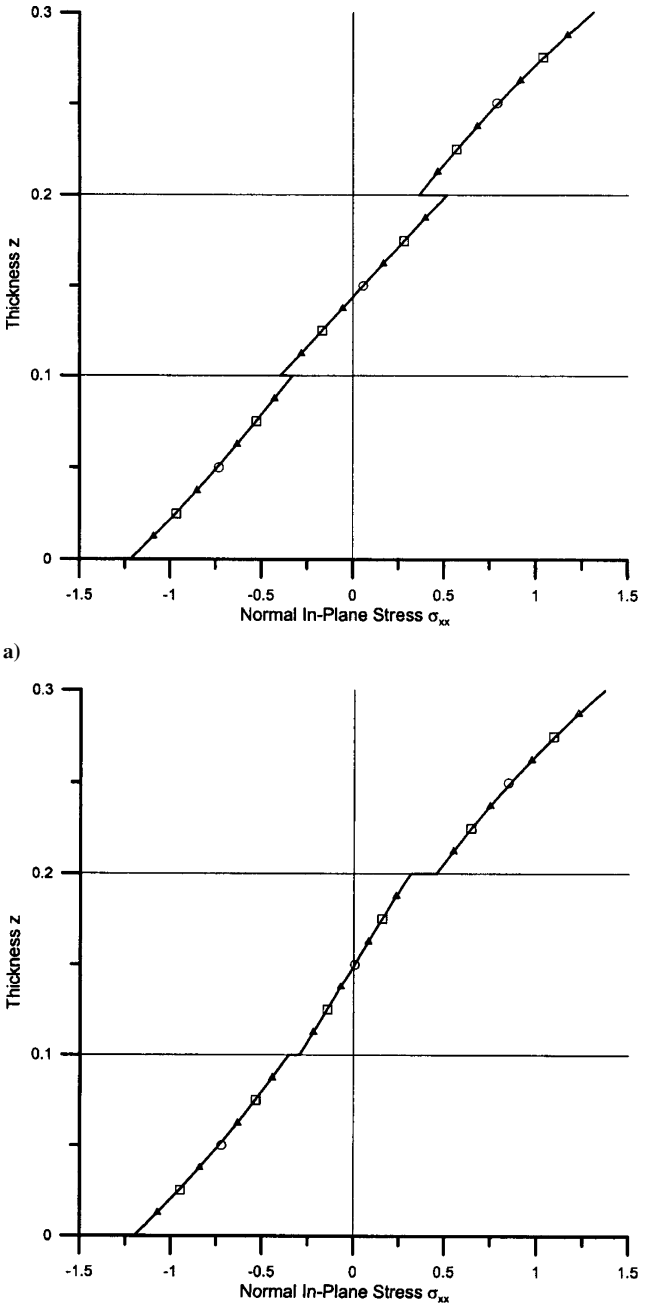

Fig. 1 In-plane normal stress σ_{xx} (in pascal) at $(L_x/2, L_y/2)$ for the three-layer laminates: a) *B*/*F*/*B* and b) *F*/*B*/*F*.

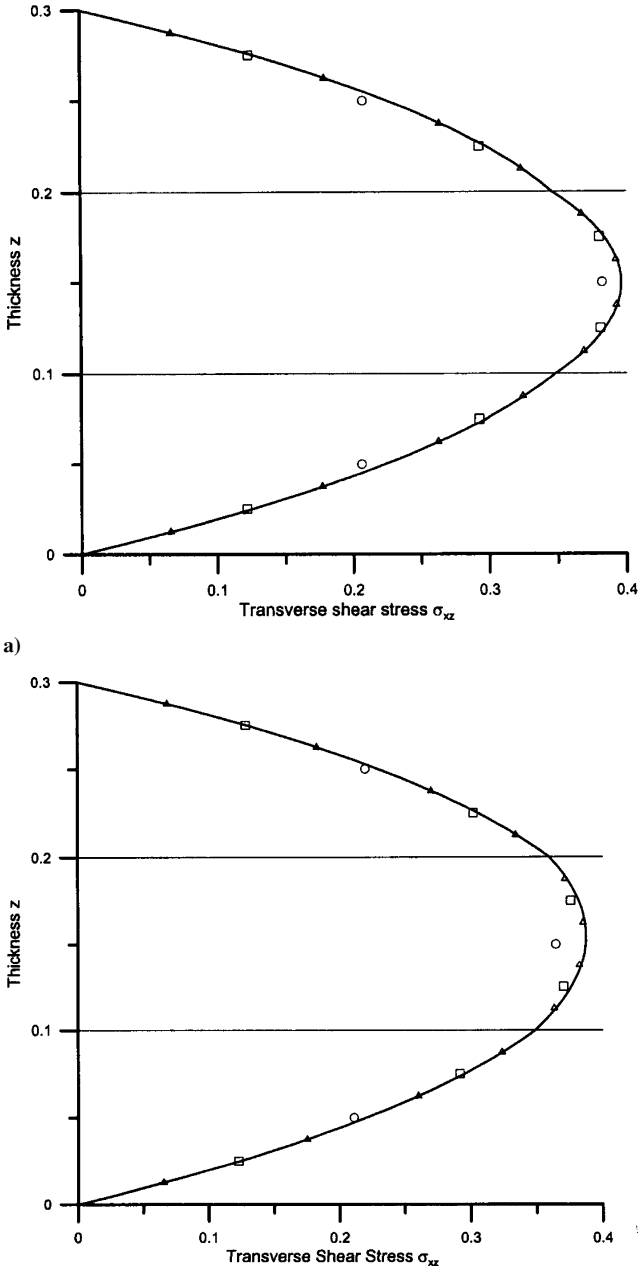

Fig. 2 Transverse shear stress σ_{xz} (in pascal) at $(0, L_y/2)$ for the three-layer laminates: a) *B*/*F*/*B* and b) *F*/*B*/*F*.

consistent with the increase in relative stiffness in going from the $BaTiO_3$ to the $CoFe_2O_4$, whereas for the $F/B/F$ laminate, there is a decrease across this interface for the same reason. In each of Figs. 1 and 2, the solid line represents both the exact solution and the present model that uses 24 or more layers, whereas the open circles, squares, and triangles represent the discrete-layer model with 3, 6, and 12 layers, respectively. In Fig. 2, the transverse shear stress component is continuous, but the dissimilar shear modulus across the interface results in a break in the shear strain and hence the z gradient of the transverse displacement. This kink in slope is slight but clear for both the $B/F/B$ and $F/B/F$ lamination schemes, with the slope either increasing or decreasing with shear modulus. Our results for the stress fields are consistent with those found by Reddy,[15] who has developed several discrete-layer models for elastic laminates. It is clear from Figs. 3 and 4 that, in terms of stress computation, a small number of layers could be used to represent the behavior of these field components through the thickness accurately, because the results for 3, 6, or 12 discrete layers are in excellent agreement with the exact solution.

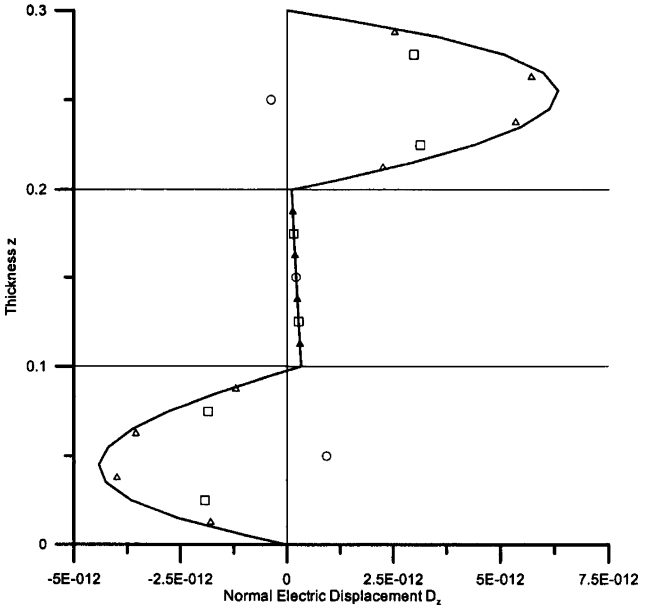

a)

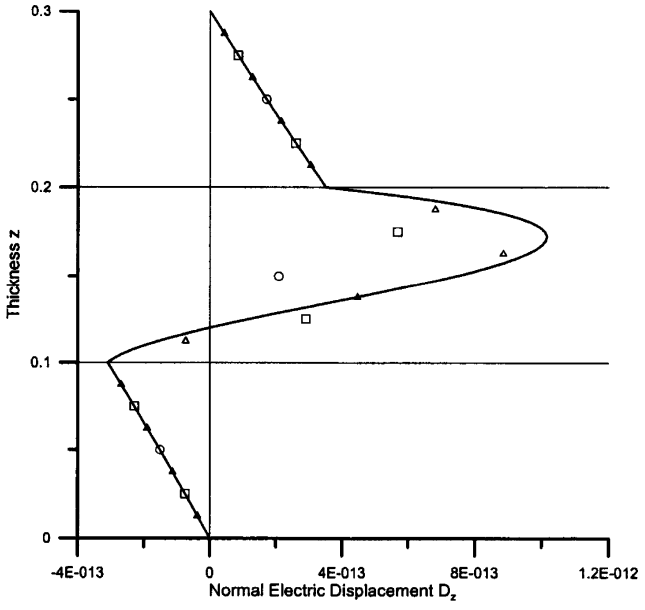

b)

Fig. 3 Normal electric displacement D_z (in coulombs per square meter) at ($L_x/2$, $L_y/2$) for the three-layer laminates: a) $B/F/B$ and b) $F/B/F$.

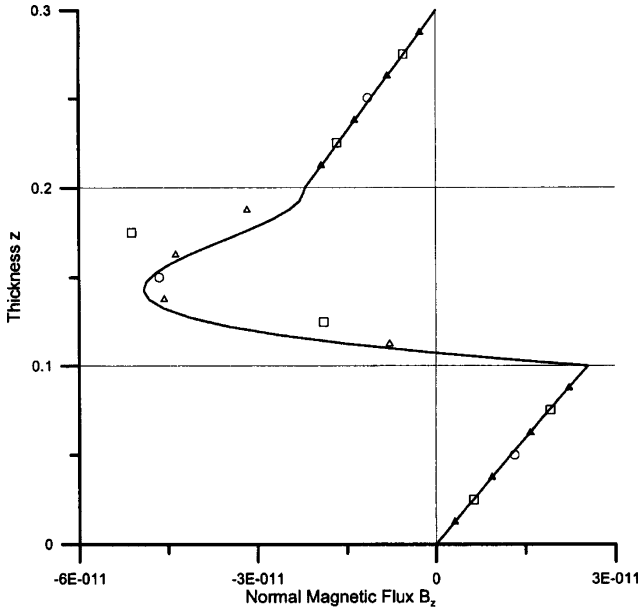

a)

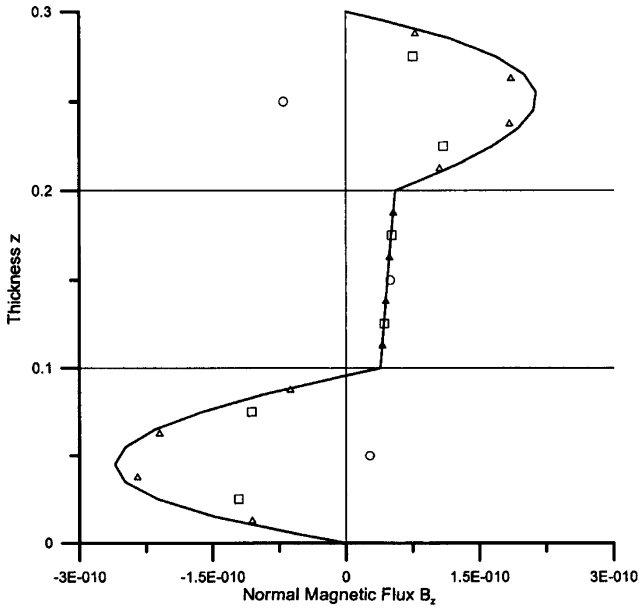

b)

Fig. 4 Normal magnetic flux component B_z (in newtons per ampere meter) at ($L_x/2$, $L_y/2$) for the three-layer laminates: a) $B/F/B$ and b) $F/B/F$.

In Figs. 3 and 4, the transverse components of the electric displacement and the magnetic flux are shown as a function of laminate thickness. Here the mismatch in properties is even more significant because crossing the interface results in going from a piezoelectric medium to a magnetostrictive medium (and vice versa), with the magnetostrictive and piezoelectric coefficients going from zero to nonzero (and vice versa). However, the field behavior in these two types of layers is very similar because of the nature of the coupling with the electric and magnetic field, and the resulting through-thickness fields reflect this similarity.

The normal component of the electric displacement is shown in Fig. 3 for the $B/F/B$ and $F/B/F$ lamination schemes, and the normal component of magnetic flux is shown in Fig. 4. Two features of these curves are especially apparent. First, the electric displacement in the magnetostrictive layer and the magnetic flux in the piezoelectric layer are effectively linear, with these patterns reversed for the magnetic flux in the piezoelectric layer and the electric displacement in the magnetostrictive layer, as shown in Figs. 3 and 4. Second, the magnetic flux in the magnetostrictive layer and the electric displacement in the piezoelectric layer are highly nonlinear (with a similar reversal of pattern in the $B/F/B$ and $F/B/F$ laminates), with this behavior varying so dramatically that the field quantities given by three and six discrete layers are poor approximations of the true field behavior. Only for the case of 12 layers are these quantities well-represented and even close to the exact solution. This behavior is in direct contrast to the elastic stress fields, for which even three layers gives excellent results. Hence for a laminate with the aspect ratio considered here ($L/h = 3.33$), a minimal number of layers, that is, one, may be adequate to represent the three displacement components and the respective in-plane stress fields for each layer of the laminate, but at least four layers or a third-order sublayer polynomial may be required to adequately represent the electric and magnetic potentials.

Influence of Aspect Ratio

In nearly all plate theories, the behavior of the field variables changes dramatically as the plate aspect ratio increases. For elastic

laminates, the displacement components tend to approach the kinematic behavior of Kirchhoff plate theory and the stress fields tend to become smooth through the laminate thickness. We investigate this dependence for the three-layer magnetoelelectroelastic laminate considered in the preceding section for the same static loading as in the preceding section. The laminate thickness is fixed as before, but the side lengths of the plate are changed to vary the L/h ratio. Of interest here is the nature of the electric and magnetic potentials as the laminate becomes thin. The field behavior is plotted by normalizing against the maximum value of the electric potential ϕ or the magnetic potential ψ through the laminate thickness for five aspect ratios: 2, 4, 6, 10, and 50. A total of 60 layers (20 per physical layer) are used to compute the fields through the thickness.

The results of these analyses are shown in Fig. 5 for the $B/F/B$ laminate and Fig. 6 for the $F/B/F$ laminate. In Figs. 5 and 6, the short-dashed, medium-dashed, long-dashed, and dash–dot lines are used to show field behavior for aspect ratios of 2, 4, 6, and 10. The solid line represents the behavior for the very thin plate with aspect ratio of 50.

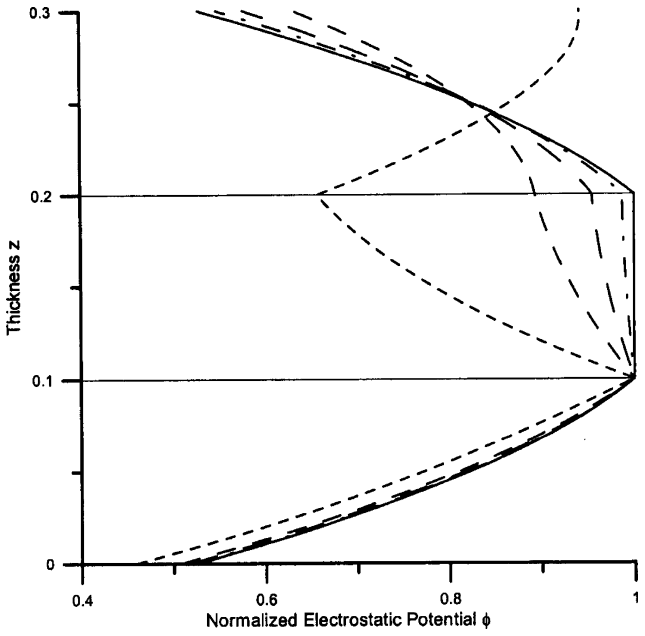

a) Electric potential for *B*/*F*/*B*

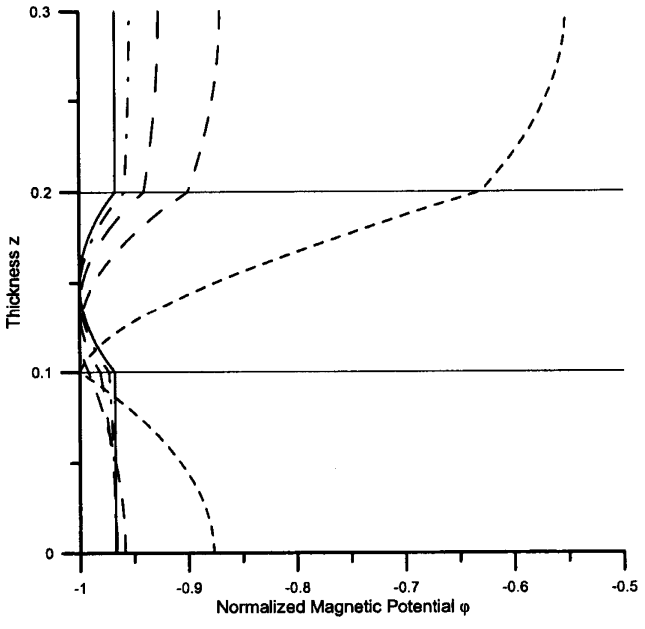

b) Magnetic potential for *B*/*F*/*B*

Fig. 5 Through-thickness dependence of a) electric potential and b) magnetic potential at (L_x/2, L_y/2) on laminate aspect ratio for the *B*/*F*/*B* lamination scheme.

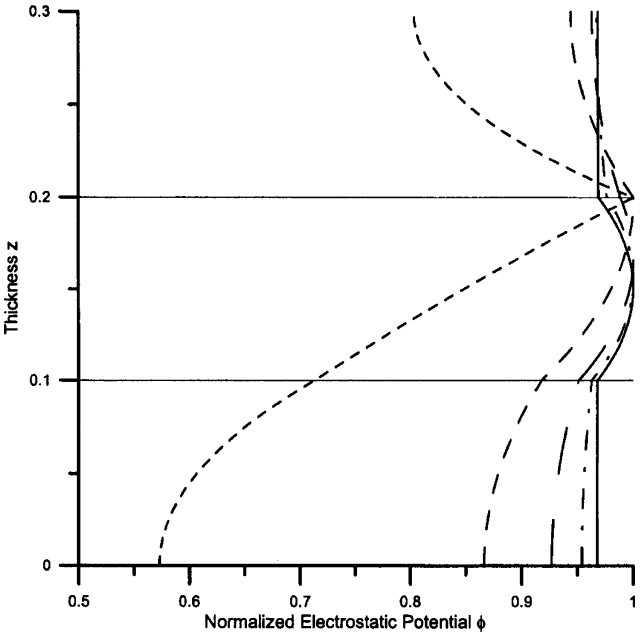

a) Electric potential for *F*/*B*/*F*

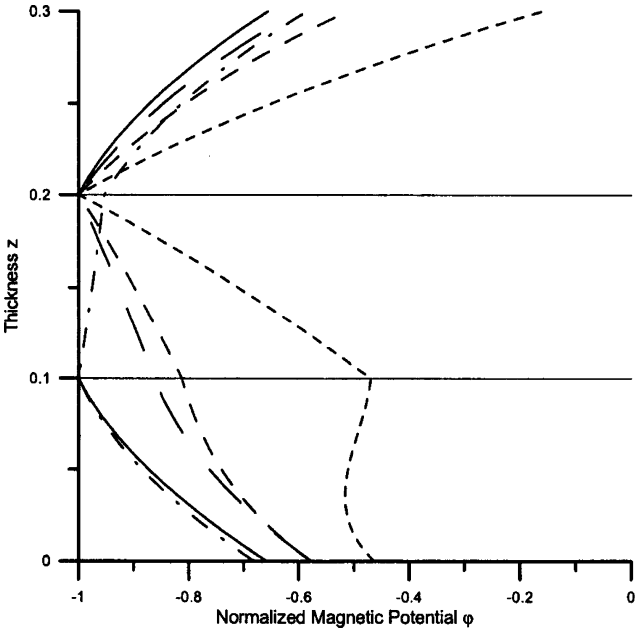

b) Magnetic potential for *F*/*B*/*F*

Fig. 6 Through-thickness dependence of a) electric potential and b) magnetic potential at (L_x/2, L_y/2) on laminate aspect ratio for the *F*/*B*/*F* lamination scheme.

The through-thickness characteristics depend strongly on aspect ratio but quickly tend to a very specific behavior as the aspect ratio increases. The electric potential in the $B/F/B$ laminate and the magnetic potential in the $F/B/F$ laminate both go from a strongly unsymmetric zig–zag behavior for $L/h = 2$ but then quickly tend toward a symmetric shape that is only mildly nonlinear in the outer layers and constant in the middle layer as the L/h ratio exceeds about 10. This behavior is consistent with the nature of the displacement fields for elastic laminates.

Completely Free Laminate

As a final example, a completely traction-free laminate is considered with applied surface potential. The laminate is a two-layer

Table 9 Through-thickness values of all variables at positive corner of laminate for completely free bimaterial under specified surface magnetic potential for discrete-layer and finite element models

z	U (DL)	U (FE)	W (DL)	W (FE)	ϕ (DL)	ϕ (FE)	ψ (DL)	ψ (FE)
$-H/2$	$-0.367e-10$	$-0.361e-10$	$0.964e-10$	$0.976e-10$	-0.00754	-0.00773	0.0	0.0
$-H/4$	$-0.319e-10$	$-0.319e-10$	$0.384e-10$	$0.398e-10$	-0.00708	-0.00743	0.0296	0.0296
0	$-0.185e-10$	$-0.185e-10$	$-0.243e-10$	$-0.233e-10$	-0.00321	-0.00364	0.0592	0.0592
$H/4$	$-0.165e-10$	$-0.162e-11$	$-0.197e-10$	$-0.182e-10$	0.00139	0.00129	0.5296	0.5296
$H/2$	$0.377e-11$	$0.318e-11$	$-0.175e-10$	$-0.157e-10$	0.0	0.0	1.00	1.0

Table 10 Field values at positive corner of bimaterial laminate with varying ratio of individual layer thicknesses

H_2/H_1	u_{top}	u_{bot}	w_{top}	w_{bot}	ϕ_{int}	ϕ_{bot}	ψ_{int}
1	$0.377e-11$	$-0.367e-10$	$-0.175e-10$	$0.964e-10$	-0.00321	-0.00773	0.0592
3	$-0.960e-12$	$-0.624e-10$	$-0.467e-10$	$0.285e-9$	0.00845	-0.0138	0.1588
9	$-0.511e-10$	$-0.115e-9$	$-0.479e-10$	$0.673e-9$	-0.00037	-0.0225	0.3615
$H = H_2$	$-0.283e-9$	$-0.283e-9$	$-0.940e-9$	$0.940e-9$	0.0	0.0	0.5

square plate of total thickness H, with a layer of $BaTiO_3$ layer on the top with thickness h_1, and a layer of $CoFe_2O_4$ on the bottom with thickness h_2. Over the upper surface of the plate the magnetic potential is fixed at one, and the bottom surface of the plate is fixed at zero magnetic potential. All surfaces of the plate are traction free, with the plate edges further experiencing zero normal electric displacement and magnetic flux. The top of the laminate is also fixed at zero electric potential, with zero normal electric displacement at the bottom.

For this set of boundary conditions, the approximation functions are different from those used in the preceding section, and this problem also differs in that there is not an exact solution with which to compare. However, it is a useful geometry to study because it gives an example of a smart component that can sense (or actuate) both electric and magnetic fields. The in-plane functions for each of the variables are selected as power series in x and y, with the general form of these in-plane functions being given as

$$\Gamma_{nm} = x^m y^n \tag{13}$$

where, for this example, the origin for (x, y) is shifted to the plate center for simplicity. The through-thickness approximation functions remain as in the preceding case. Hence, the coefficients of the functions corresponding to the electric potential on the top surface of the plate are each forced to be zero (with the exception of the single functions where $m = n = 0$), thereby enforcing the uniform potential on this surface. The bulk of the boundary conditions are of the natural type, and are, therefore, satisfied in an integral sense over each of these surfaces. To eliminate the rigid-body modes of the laminate, we specify $u = v = w = 0$ at the interface location between the two dissimilar layers at the center of the x–y plane of the laminate and also select basis functions for the five field quantities that have the proper symmetry for this loading condition.

We select four layers (two for each material) and a total of four in-plane terms to analyze this laminate, yielding a resulting linear system with 100 unknowns (five layer interface locations times four in-plane approximations times five variables). The (x, y) functions are power series that are the lowest order functions possible that meet symmetry conditions. For example, the u-displacment component is odd in x and even in y, and, hence, these functions are used: x, xy^2, x^3, and x^3y^2. Similar functions are used for v with the x and y dependence switched. For w and the two potentials, the functions are even in both spatial variables. Hence, we use one, x^2, y^2, and x^2y^2.

Several layer thicknesses are considered by the use of the fixed side lengths of 0.02 m in all three directions. First, equal thicknesses of the two differing material layers are considered. We compare these results with a three-dimensional finite element calculation using 16 eight-noded brick elements[16] to model one quadrant of the plate using symmetry conditions. The results of our analysis are shown in Table 9, with good agreement found between these two approaches. We then vary the ratio of the thickness of the two layers by making the upper layer of the piezoelectric material thinner. Hence, the total thickness is kept fixed at $h = 0.02$, but we vary the ratio of layer thicknesses, considering the values of 1, 3, and 9 for h_2/h_1. The results are shown in Table 10 for the extreme positive point on the laminate, that is, $x = y = 0.01$ m, for the u and w displacements at the top and bottom of the laminate, the electric potential at the dissimilar interface and the bottom of the laminate, and the magnetic potential at the same interface. The vertical displacement at the bottom of the laminate continues to increase as the upper layer of the laminate becomes thin, and in each case the displacements and the potential values result from both the individual layers and their interactions because of the mismatch in material properties. For comparison, we also show the field quantities when the entire block is formed of the magnetostrictive material; clearly, in this case, the displacements at the top and bottom of the laminate reflect the material symmetry, and the magnetic potential is perfectly linear with the three constant displacements corresponding to the exact magnetostrictive behavior one would find in the absence of stress within the block. (Showing results for a block of pure piezoelectric material in this case would also give a perfectly linear magnetic potential distribution, but all other field quantities would be identically zero.) In the present case, the tendency of the three normal strains in the lower layer is negative because the dominant magnetic field component in the thickness direction is negative. As the upper layer becomes smaller, the bending behavior induced by the material mismatch tends more toward a pure negative normal strain in all three directions. These combined electromagnetoelastic composites could be formed for use in both sensing and actuating situations where either one or both electric and magnetic fields may be present or require detection. Our intent of this example is merely to show an example of the relative change in field quantities, and more specific applications and parametric studies of such devices await future examination.

Summary

In this study, the static behavior of laminates with coupled elastic, electric, and magnetic behavior are considered by the use of a discrete-layer approximate model that explicitly accounts for discontinuities of slope of the displacement field, the electric field, and the magnetic field. Homogeneous and laminated media were considered under the conditions of simple support. These sets of constraints are considered primarily because exact solutions exist for these solids, and they provide a good means of comparison.

Several test geometries were considered: the simply supported laminate, for which an exact solution exists for comparison, and the completely free laminate. For even a fairly small number of layers in the simply supported geometry, errors between the approximate model and the exact solution were within several percent. For the completely free composite, we compare our discrete-layer model

with a three-dimensional finite element calculation with excellent agreement and demonstrate the level of coupling in a simple bimaterial laminate with potential sensing and actuating applications.

We also found that the behavior of the potential functions is similar to that of elastic plate field quantities, in that when the aspect ratio exceeds approximately 10, the electric and magnetic potentials tend nearly to constant/linear behavior in the two types of material layers. Hence, it appears to be quite possible to develop a simplified plate model by the use of a fairly small number of through-thickness unknowns that can accurately capture interlaminar stress and electric and magnetic flux quantity behaviors.

Appendix: Element Matrices

The form of the element matrices can be expressed in compact form, especially when the approximation functions are kept in terms of all three spatial variables, (that is, before the actual discrete-layer approximation splits the form of these functions into out-of-plate (z) dependence and in-plane (x–y) dependence. In application, the z dependence is preintegrated out of the approximation, leaving only the x–y operators in the element matrices.

Constitutive laws more general than those considered here are easily implemented in the model used in this study. The element stiffness matrices follow:

$$K_{11}^{ij} = \int_V \left(C_{11}\frac{\partial\Gamma_i^u}{\partial x}\frac{\partial\Gamma_j^u}{\partial x} + C_{66}\frac{\partial\Gamma_i^u}{\partial y}\frac{\partial\Gamma_j^u}{\partial y} + C_{55}\frac{\partial\Gamma_i^u}{\partial z}\frac{\partial\Gamma_j^u}{\partial z} \right) \mathrm{d}V$$

$$K_{12}^{ij} = \int_V \left(C_{12}\frac{\partial\Gamma_i^u}{\partial x}\frac{\partial\Gamma_j^v}{\partial y} + C_{66}\frac{\partial\Gamma_i^u}{\partial y}\frac{\partial\Gamma_j^v}{\partial x} \right) \mathrm{d}V$$

$$K_{13}^{ij} = \int_V \left(C_{13}\frac{\partial\Gamma_i^u}{\partial x}\frac{\partial\Gamma_j^w}{\partial z} + C_{55}\frac{\partial\Gamma_i^u}{\partial z}\frac{\partial\Gamma_j^w}{\partial x} \right) \mathrm{d}V$$

$$K_{14}^{ij} = \int_V \left(e_{31}\frac{\partial\Gamma_i^u}{\partial x}\frac{\partial\Gamma_j^\phi}{\partial z} + e_{15}\frac{\partial\Gamma_i^u}{\partial z}\frac{\partial\Gamma_j^\phi}{\partial x} \right) \mathrm{d}V$$

$$K_{15}^{ij} = \int_V \left(q_{31}\frac{\partial\Gamma_i^u}{\partial x}\frac{\partial\Gamma_j^\psi}{\partial z} + q_{15}\frac{\partial\Gamma_i^u}{\partial z}\frac{\partial\Gamma_j^\psi}{\partial x} \right) \mathrm{d}V$$

$$K_{22}^{ij} = \int_V \left(C_{66}\frac{\partial\Gamma_i^v}{\partial x}\frac{\partial\Gamma_j^v}{\partial x} + C_{22}\frac{\partial\Gamma_i^v}{\partial y}\frac{\partial\Gamma_j^v}{\partial y} + C_{44}\frac{\partial\Gamma_i^v}{\partial z}\frac{\partial\Gamma_j^v}{\partial z} \right) \mathrm{d}V$$

$$K_{23}^{ij} = \int_V \left(C_{23}\frac{\partial\Gamma_i^v}{\partial y}\frac{\partial\Gamma_j^w}{\partial z} + C_{44}\frac{\partial\Gamma_i^v}{\partial z}\frac{\partial\Gamma_j^w}{\partial y} \right) \mathrm{d}V$$

$$K_{24}^{ij} = \int_V \left(e_{32}\frac{\partial\Gamma_i^v}{\partial y}\frac{\partial\Gamma_j^\phi}{\partial z} + e_{24}\frac{\partial\Gamma_i^v}{\partial z}\frac{\partial\Gamma_j^\phi}{\partial y} \right) \mathrm{d}V$$

$$K_{25}^{ij} = \int_V \left(q_{32}\frac{\partial\Gamma_i^v}{\partial y}\frac{\partial\Gamma_j^\psi}{\partial z} + q_{24}\frac{\partial\Gamma_i^v}{\partial z}\frac{\partial\Gamma_j^\psi}{\partial y} \right) \mathrm{d}V$$

$$K_{33}^{ij} = \int_V \left(C_{55}\frac{\partial\Gamma_i^w}{\partial x}\frac{\partial\Gamma_j^w}{\partial x} + C_{44}\frac{\partial\Gamma_i^w}{\partial y}\frac{\partial\Gamma_j^w}{\partial y} + C_{33}\frac{\partial\Gamma_i^w}{\partial z}\frac{\partial\Gamma_j^w}{\partial z} \right) \mathrm{d}V$$

$$K_{34}^{ij} = \int_V \left(e_{15}\frac{\partial\Gamma_i^w}{\partial x}\frac{\partial\Gamma_j^\phi}{\partial x} + e_{24}\frac{\partial\Gamma_i^w}{\partial y}\frac{\partial\Gamma_j^\phi}{\partial y} + e_{33}\frac{\partial\Gamma_i^w}{\partial z}\frac{\partial\Gamma_j^\phi}{\partial z} \right) \mathrm{d}V$$

$$K_{35}^{ij} = \int_V \left(q_{15}\frac{\partial\Gamma_i^w}{\partial x}\frac{\partial\Gamma_j^\psi}{\partial x} + q_{24}\frac{\partial\Gamma_i^w}{\partial y}\frac{\partial\Gamma_j^\psi}{\partial y} + q_{33}\frac{\partial\Gamma_i^w}{\partial z}\frac{\partial\Gamma_j^\psi}{\partial z} \right) \mathrm{d}V$$

$$K_{44}^{ij} = \int_V \left(-\varepsilon_{11}\frac{\partial\Gamma_i^\phi}{\partial x}\frac{\partial\Gamma_j^\phi}{\partial x} - \varepsilon_{22}\frac{\partial\Gamma_i^\phi}{\partial y}\frac{\partial\Gamma_j^\phi}{\partial y} - \varepsilon_{33}\frac{\partial\Gamma_i^\phi}{\partial z}\frac{\partial\Gamma_j^\phi}{\partial z} \right) \mathrm{d}V$$

$$K_{45}^{ij} = \int_V \left(-d_{11}\frac{\partial\Gamma_i^\phi}{\partial x}\frac{\partial\Gamma_j^\psi}{\partial x} - d_{22}\frac{\partial\Gamma_i^\phi}{\partial y}\frac{\partial\Gamma_j^\psi}{\partial y} - d_{33}\frac{\partial\Gamma_i^\phi}{\partial z}\frac{\partial\Gamma_j^\psi}{\partial z} \right) \mathrm{d}V$$

$$K_{55}^{ij} = \int_V \left(-\mu_{11}\frac{\partial\Gamma_i^\psi}{\partial x}\frac{\partial\Gamma_j^\psi}{\partial x} - \mu_{22}\frac{\partial\Gamma_i^\psi}{\partial y}\frac{\partial\Gamma_j^\psi}{\partial y} - \mu_{33}\frac{\partial\Gamma_i^\psi}{\partial z}\frac{\partial\Gamma_j^\psi}{\partial z} \right) \mathrm{d}V$$

Acknowledgment

Part of this study was initiated when the first author was an Alexander von Humboldt Research Fellow at the University of Stuttgart. The support of the Alexander von Humboldt Research Foundation is gratefully acknowledged.

References

[1]Saravanos, D. A., and Heyliger, P. R., "Mechanics and Computational Models for Laminated Piezoelectric Beams, Plates, and Shells," *Applied Mechanics Reviews*, Vol. 52, 1999, pp. 305–320.

[2]Tzou, H. S., *Piezoelectric Shells: Distributed Sensing and Control of Continua*, Kluwer Academic, Norwell, MA, 1993.

[3]Harshe, G., Dougherty, J. P., and Newnham, R. E., "Theoretical Modeling of Multilayer Magneoelectric Composites," *International Journal of Applied Electromagnetics*, Vol. 4, 1993, pp. 145–159.

[4]Nan, C. W., "Magnetoelectric Effect in Composites of Piezoelectric and Piezomagnetic Phases," *Physical Review B*, Vol. 50, 1994, pp. 6082–6088.

[5]Benveniste, Y., "Magnetoelctric Effect in Fibrous Composites with Piezoelectric and Piezomagnetic Phases," *Physical Review B*, Vol. 51, 1995, pp. 16424–16427.

[6]Pan, E., "Exact Solution for Simply Supported and Multilayered Magneto-Electro-Elastic Plates," *Journal of Applied Mechanics*, Vol. 68, 2001, pp. 608–618.

[7]Pan, E., and Heyliger, P. R., "Free Vibrations of Simply-Supported and Multilayered Magneto-Electro-Elastic Plates," *Journal of Sound and Vibration*, Vol. 252, 2002, pp. 429–442.

[8]Reddy, J. N., *Energy and Variational Methods in Applied Mechanics*, Wiley, New York, 1984.

[9]Pauley, K. E., and Dong, S. B., "Analysis of Plane Waves in Laminated Piezoelectric Media," *Wave Electronics*, Vol. 1, 1976, pp. 265–285.

[10]Reddy, J. N., "A Generalization of Displacement-Based Laminate Theories," *Communications in Applied Numerical Methods*, Vol. 3, 1987, pp. 173–181.

[11]Heyliger, P., "Static Behavior of Laminated Elastic/Piezoelectric Plates," *AIAA Journal*, Vol. 32, 1994, pp. 2481–2484.

[12]Heyliger, P. R., and Saravanos, D. A., "Exact Free Vibration Analysis of Laminated Plates with Embedded Piezoelectric Layers," *Journal of the Acoustical Society of America*, Vol. 98, 1995, pp. 1547–1557.

[13]Heyliger, P. R., "Exact Solutions for Simply-Supported Laminated Piezoelectric Plates," *Journal of Applied Mechanics*, Vol. 64, 1997, pp. 299–306.

[14]Berlincourt, D. A., Curran, D. R., and Jaffe, H., "Piezoelectric and Piezomagnetic Materials and Their Function in Transducers," *Physical Acoustics*, Vol. 1, 1964, pp. 169–270.

[15]Reddy, J. N., *Mechanics of Laminated Composite Plates: Theory and Analysis*, CRC Press, Boca Raton, FL, 1997.

[16]Reddy, J. N., *Introduction to the Finite Element Method*, 2nd ed. McGraw–Hill, New York, 1993.

M. Ahmadian
Associate Editor